Preparation and Characterization of Ultrafiltration TiO_2 Nanoparticles-Polysulfone Membranes

DANIELA FLORENTINA ENACHE, GEORGE ALEXANDRU POPA, EUGENIU VASILE, ANCA RAZVAN, OVIDIU OPREA, ELENA VOICILA, FLORINA DUMITRU*
University Politehnica of Bucharest, 1-7 Polizu Str., 011061,Bucharest, Romania

This paper presents the preparation route for new TiO_2 nanoparticles-polysulfone membranes: M1 (Psf 12%), M2 (Psf 12% + TiO_2 anatase), and M3 (Psf 12% + TiO_2 76% anatase + 24% rutile) that were structurally characterized by FTIR, TG-DSC and by scanning electron microscopy (SEM) coupled with energy dispersive spectroscopy (EDAX). Contact angle measurements, dead-end and cross-flow filtration experiments were carried out to characterize the morphology and hydrodynamic performance of the prepared membranes. Improved mechanical properties, enhanced hydrophilicity and the relative large water flux measured for M2-M3 (721.83 L/m²·h and 305.4 L/m²·h, respectively) in cross-flow filtration experiments, make these membranes appropriate for ultrafiltration applications.

Keywords: TiO_2 nanoparticles, polysulfone, blend membranes, ultrafiltration

The incorporation of inorganic nanoparticles into a polymeric matrix endows the material with multifunctional properties, hydrophilicity, mechanical strength, high water permeability, high retention rate and enhanced antifouling resistance. Therefore, in most wastewater treatment processes, the nanoparticles incorporated into membranes are inorganic oxides: MgO, Fe_3O_4, Al_2O_3, TiO_2, SiO_2, ZnO, Fe_2O_3, metals (*e.g.* Cu^0, Ag^0) or carbon-based materials (*e.g.* graphene and carbon nanotubes) [1-13].

Among these nanoparticles, the nanometric-sized TiO_2 having photocatalytic and antibacterial activity are very effective as surface hydrophilicity modifiers, thus reducing the membrane fouling with organic matter and augmenting the water flux through membrane [14-23]. The superhydrophilic surface of TiO_2 together with the nanometer dimensions of the particles are the main properties considered in the design of nanocomposite membranes [24-31].

Jyothi et al. [32, 33] prepared polysulfone Psf/TiO_2 composite membranes and studied the rejection of chromium oxospecies (*i.e.* $HCrO_4^-$ and $HCr_2O_7^-$) by these membranes. For a Psf membrane modified with 2% wt TiO_2 nanoparticles (TiO_2 NPs), the rejection of Cr(VI) reaches maximum value at *p*H=2.

Yang et al. [34-36] assessed the efficiency of a TiO_2/Psf composite membrane in kerosen emulsified wastewater treatment and they showed that embedded TiO_2 nanoparticles (2% wt, 20-30 nm diameters) improved the membrane performance in terms of hydrophilicity and antifouling characteristics. According to these studies, the optimum concentration of TiO_2 nanoparticles in blend membrane is 2% wt; above this concentration the blending mixture (polymer-nanoparticles) become more viscous and TiO_2 nanoparticles form aggregates onto the membrane surface. For TiO_2 NPs concentrations ranging from 1% to 5% wt in blending mixture, the pore density increases from 690 pores/îm² (TiO_2 1%) to 1130 pores/μm² (TiO_2 5%) and the membrane surface porosity increases from 60.3% (TiO_2 1%) to 85.7% (TiO_2 5%) [34-36].

Another important factor in tuning the membrane hydrodynamic performances is represented by the particle size of TiO_2 polymorphs: anatase TiO_2 with particle average diameter ~ 10-20 nm are reported to have a better antifouling effect when used as membrane inorganic nanofiller then larger rutile TiO_2 nanoparticles (average diameter ~ 30 nm) [37, 38].

Taking into consideration the results in designing polymer/TiO_2 nanocomposite membranes, we prepared TiO_2/Psf membranes with anatase and rutile nanofillers and we characterized these membranes both structurally (FTIR, TG-DSC, SEM/EDAX), and hydrodynamically, by contact angle measurements and water flux experiments. The crystalline structure of TiO_2 was assigned either to anatase or rutile phase by powder XRD analysis and the corresponding particles diameters have been estimated with Debye-Scherrer equation.

Experimental part

Techniques and materials

All reagents and solvents were commercially available and used as received. Polysulfone (BASF, ULTRASON® - S-2010, white powder, 1.24 g/cm³, with low viscosity in organic solvents, 50mL/g, 25°C, and an average molecular weight of 40000 Da) has been used as polymer support.

FTIR vibrational spectra were recorded with a Bruker Tensor 27 spectrophotometer, with the ATR sampling unit, in the wavenumbers range of 500-4000 cm^{-1}.

The electronic (UV-Vis) spectra were recorded at the room temperature on a Jasco V560 in the diffuse reflectance technique.

Thermal analysis TG-DSC was carried out with a Netzsch 449C STA Jupiter. Samples were placed in open Al_2O_3 crucible and heated with 10 degrees·min^{-1} from room temperature to 900°C, under the flow of 20 mL·min^{-1} dried air. An empty Al_2O_3 crucible was used as reference.

Powder X-ray diffraction (PXRD) patterns were recorded on a Panalytical X'PERT PRO MPD diffractometer with graphite monochromatized CuKα radiation (λ=1.5418 Å). The samples were scanned in the Bragg angle, 2θ range of 15-90°.

SEM images were recorded on a SEM/EDAX High Resolution Scanning Electron Microscope, Quanta Inspect F FEG (resolution 1.4nm) with EDAX (133 eV resolution at MnKα) – FEI Company.

* email: florina.dumitru@upb.ro;

Contact angle measurements were carried out with Contact Angle Meter – KSV Instruments CAM 100. Each contact angle value represents the average of a minimum of 5 measurements.

Dead-end and cross-flow filtration experiments were carried out to characterize the performance of the prepared membranes. The ultrafiltration experiments were conducted using a laboratory-scale dead-end (**DE**) and cross-flow (**CF**) filtration system (equipped with a variable speed driven centrifugal pump: Q= 40 L/min, n=287 rpm, and H_{max} = 4 bar) at temperature of 25°C and pressures of 0.5, 1, 2, 2.5 and 3 bar. For each type of membrane, the water flux was determined by measuring the collecting time for the volume of 100 mL of permeate. The membranes diameter was 36 mm. The permeate volume was determined on steady flow conditions. The flux (J), defined as the flow rate of water passing through the membrane, per unit area of membrane, was calculated using the formula: $J = \frac{Q_p}{A_m}$ [L/m²·h], where: Q_p = filtrate flow rate through membrane [L/h], A_m = surface area of membrane [m²].

Preparation of TiO_2 NPs

TiO_2 NPs have been prepared as described in [39], slightly modified. 5g $TiOSO_4$ were dispersed in 100 mL hot distilled water and, while maintaining the mixture under vigorous stirring, 25 % wt ammonia solution was added until *p*H = 7. The basic hydrolysis of $TiOSO_4$ lead to hydrated titanium oxide, $TiO_2 \cdot xH_2O$. After copious washing with water, $BaCl_{2\,(aq)}$ test for SO_4^{2-} was performed; the white precipitate, free of sulfate ion, was dried in oven at 60°C, for 24 h.

The as-synthesised TiO_2 – as anatase polymorph was susequently calcined at 900°C for 3h, for obtaining the rutile polymorph.

Preparation of membranes

Polysulfone solutions of 12% wt concentration in dimethylformamide (DMF) were obtained in borosilicate glass vials with polyester caps, under stirring at room temperature for 24 h.

The blending mixture TiO_2 (1% wt)-polysulfone (12%)-DMF was cast in a thin film of 0.4 mm on a glass plate using a film casting device. Deionized water was used as coagulation agent (bath temperature, 25°C). Hence, the membranes **M1 =** Psf 12% - reference membrane, **M2** = Psf 12% + TiO_2 (anatase), and **M3** = Psf 12% + TiO_2 (thermal treated) were obtained.

Results and discussions

TiO_2 nanoparticles

FTIR spectra

To assess the formation of TiO_2 from $TiOSO_4$ subjected to basic hydrolysis, FTIR spectra in the 500-4000 cm^{-1} wavelength range were performed (fig. 1). In the FTIR spectrum of $TiOSO_4 \cdot xH_2O$, absorption peaks corresponding to the stretching vibration of SO_4^{2-} around 990-1200 cm^{-1} (990, 1065, and 1140 cm^{-1}) are present. The sulfate ions, SO_4^{2-}, act as bidentate ligands toward Ti^{4+} (TiO^{2+}) ions. In the FTIR spectra of both TiO_2 (*as-synthesized*) and TiO_2 (*thermal treated*) these peaks were no longer present and the spectra indicate the formation of the more symmetric crystalline compounds, with broad vibration bands in the 600-900 cm^{-1} wavelength range, which can be attributed to the newly formed O-Ti-O-Ti bonds. The absorption peak at 1414 cm^{-1} can be assigned to the bending vibration

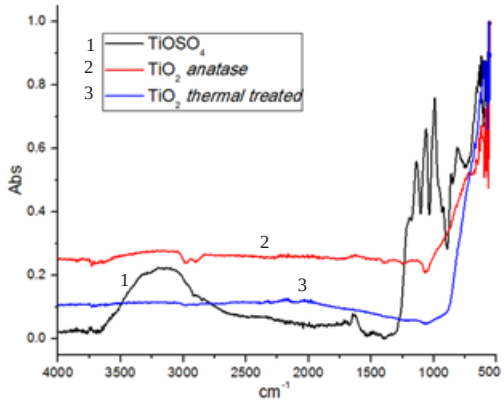

Fig. 1. FTIR spectra of $TiOSO_4$, TiO_2 anatase (*as-synthesized*) and TiO_2 (*thermal treated*)

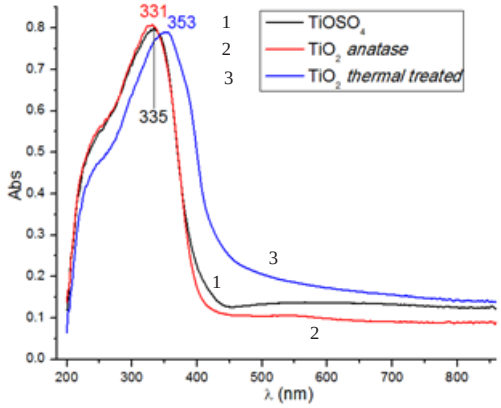

Fig. 2. UV-Vis spectra of $TiOSO_4$, TiO_2 anatase (*as-synthesized*) and TiO_2 (*thermal treated*)

($\delta_{H\text{-}O\text{-}H}$) from water molecules adsorbed onto the surface of TiO_2 nanopowders.

UV-Vis spectra

TiO_2 NPs were extensively studied for their photocatalytic and antibacterial properties and it is a known fact that the energy gap is larger for TiO_2 nanoparticles of smaller dimensions.

The UV-Vis spectra (fig. 2) showed absorption maxima at 335 nm for $TiOSO_4$, 331 nm for TiO_2 anatase (*as-synthesized*), and 353 nm for TiO_2 (*thermal treated*). For these values, the energy gap ($E = hc/\lambda$, $h = 6.63 \cdot 10^{-34}$ J·s, $c = 3 \cdot 10^8$ m/s, 1eV = $1.6 \cdot 10^{-19}$ J) is 3.75 eV for TiO_2 anatase (*as-synthesized*) and 3.52 eV for TiO_2 (*thermal treated*), indicating that TiO_2 (*thermal treated*) nanoparticles have, as expected, larger diameters.

PXRD

For TiO_2 (*as-synthesized*), the XRD pattern (fig. 3) corresponds to the anatase polymorph of TiO_2, as pure phase, according to the crystallographic reference 04-002-8296.

By using the Debye-Scherrer equation [40], the average diameter of the nanoparticles can be estimated:

$D = \frac{0.9\lambda}{\beta \cos\theta}$ λ = the wavelength of the CuK_α radiation = 1.5418Å or 0.15418 nm); β = FWHM (full width at half maximum); θ = diffraction angle; D = particle diameter.

Particle size calculation for TiO_2 anatase (*as-synthesized*): hkl = 101→2θ = 25.337 (I = 100%); β = (25.544-25.1618) $\cdot \frac{3.14}{180}$ = 0.0067 rad;

$$D = \frac{0.9 \cdot 0.1541}{0.0067 \cdot \cos 12.668} = 21 \text{ nm}$$

The TiO_2 powder obtained after the thermal treatment (900°C, 3h) has a XRD pattern in which diffraction peaks for both polymorphs: anatase (76%) and rutile (24%) are present (fig. 3).

Phase composition of the sample was calculated by using the equation [39]:

Rutile phase (%) = $100/[1+0.8(I_A/I_R)]$, where I_A and I_R are the 100% intensities of the anatase (hkl = 101 → 2θ = 25.38707°) and rutile (hkl = 110 → 2θ = 27.5382°) diffraction peaks, respectively.

Particle size calculation for TiO_2 anatase (76%)/TiO_2 (24%):

TiO_2 anatase hkl = 101 → 2θ = 25.38707 (I = 100%);

$$\beta = (25.5158\text{-}25.2748) \cdot \frac{3.14}{180} = 0.0042 \text{ rad}$$

$$D = \frac{0.9 \cdot 0.1541}{0.0042 \cdot cos\ 12.6935} = \mathbf{34\ nm}$$

TiO_2 rutile hkl = 110 → 2θ = 27.5382 (I = 100%);

$$\beta = (27.5938\text{-}27.4332) \cdot = 0.0028 \text{ rad}$$

$$D = \quad D = \frac{0.9 \cdot 0.1541}{0.0042 \cdot cos\ 12.6935} = \mathbf{51\ nm}$$

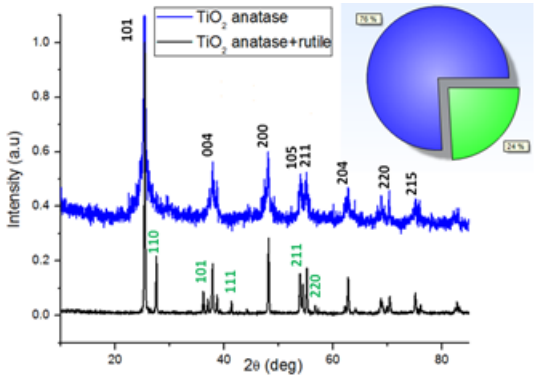

Fig. 3. XRD pattern of TiO_2 anatase (*as-synthesized*) and TiO_2 anatase + rutile (*thermal treated*)

As seen from figure 3, broad diffraction peaks are observed for TiO_2 anatase indicating the formation of small nanoparticles, while for TiO_2 mixed phase (76% anatase, 24% rutile) the diffraction peaks are sharper, better defined, as a result of the increase of crystallinity and crystal size upon the thermal treatment. The temperature (900°C) has a significant effect on the crystallite size TiO_2 anatase, the particle size increase from ~21 nm to ~34 nm.

TiO_2/Psf membranes

The **M1** (Psf 12%), **M2** (Psf 12% + TiO_2 anatase), and **M3** (Psf 12% + TiO_2 76% anatase + 24% rutile) membranes were prepared by phase-inversion method [40-47].

The nanoparticles (1% wt either TiO_2 anatase or TiO_2 76% anatase + 24% rutile) were blended with polysulfone solution (12%wt) in DMF and then cast onto a glass plate. The nanocomposite membranes were formed by dipping this glass plate in deionized water, the non-solvent for the polysulfone polymer.

FTIR spectra

In the FTIR spectra of **M1-M3** membranes (fig. 4), only the absorption maxima attributed to the structure of polysulfone: 1104 cm^{-1} (C-O), 1149 cm^{-1} (R(SO_2)-R), 1239 cm^{-1} (C-O), 1488 cm^{-1} (C=C aromatic), 2921 cm^{-1} (CH alifatic), 2965 cm^{-1} (CH aromatic) and 3367 cm^{-1} (OH), respectively, have been observed. The vibration bands of Ti-O bond appear in the 600-900 cm^{-1} range and they are probably obscured by the peaks of polysulfone.

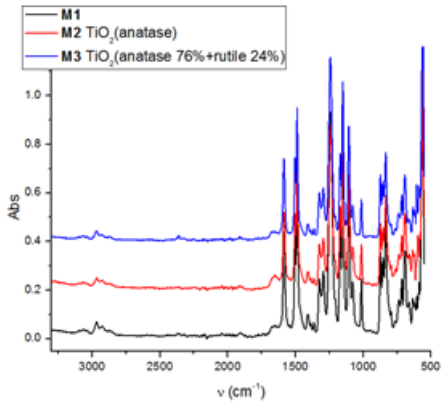

Fig. 4. FTIR spectra of the **M1-M3** membranes

- Thermal analysis (TG-DSC)

The thermal analysis curves (TG-DSC) for **M1-M3** membranes are depicted in figure 5 (a) and (b).

The total experimental mass loss is 91.02% wt for **M1**, 88.84% wt for **M2** and 93.06% wt for **M3**, respectively.

The DSC curves are very similar in shape for all three membranes, and they present:

- two moderate exothermic effects, 420°C < T < 540°C, attributed to the beginning of the decomposition process of polysulfone polymer,

- one strong exothermic effect centered at 607°C for **M1** (Psf 12%), at 616°C for **M2** (Psf 12% + TiO_2 anatase), and at 627°C for **M3** (Psf 12% + TiO_2 76% anatase + 24% rutile), respectively. This effect is assigned to the combustion of polysulfone backbone.

For **M1-M3** membranes, the decomposition temperature (T_d) and the glass transition temperature (T_g) have been determined. The literature data showed that T_g and T_d for Psf membranes are 189°C and 471.95°C [35], and we found for **M1** (Psf 12%) T_g = 189.3°C and T_d = 484.1°C, values that are very close to those reported.

Generally, these temperatures are higher when inorganic nanoparticles are incorporated into material. Yang et al. [35] reported that for a TiO_2 content of 3% wt, T_d of a polysulfone membrane increased with 40.6°C (from 471.95°C/Psf to 512.55°C/Psf+TiO_2) and T_g increased with 10.2°C (from 189°C/Psf to 199.2°C/Psf+TiO_2). They attributed this behavior to the intermolecular interactions between TiO_2 NPs and polymeric chains that lead to an enhanced rigidity of polymeric film and, hence, to enhanced thermal stability of nanocomposite membrane.

M2 (Psf 12% + TiO_2 anatase) has T_g = 195.2°C and T_d = 497.1°C, both values slightly higher (with 5.9°C for T_g and 13°C for T_d) than the values determined for **M1** (Psf 12%) used as reference.

In the case of **M3** (Psf 12% + TiO_2 76% anatase + 24% rutile), the T_g = 182.3°C and T_d = 468.3°C values, lower than both **M1** and **M3** values, are, probably, the consequence of incorporating larger particles (34 nm/anatase and 51 nm/rutile as estimated by PXRD) in blending mixture and thus inducing the macropores formation in the membrane.

Scanning electron microscopy SEM/EDAX

To obtain insights into membranes morphologies [49-51], cross-section structures of **M1-M3** were visualized by SEM (figs. 6 and 7 (a)). Cross-section images of the membranes showed very similar morphologies, but for **M2** (Psf 12% + TiO_2 anatase) and **M3** (Psf 12% + TiO_2 76% anatase + 24% rutile) the asymmetry of the membranes was apparent, as a result of the addition of TiO_2 NPs to the membranes. For **M3**, the blending of larger TiO_2 NPs with polysulfone in the casting suspension caused the formation

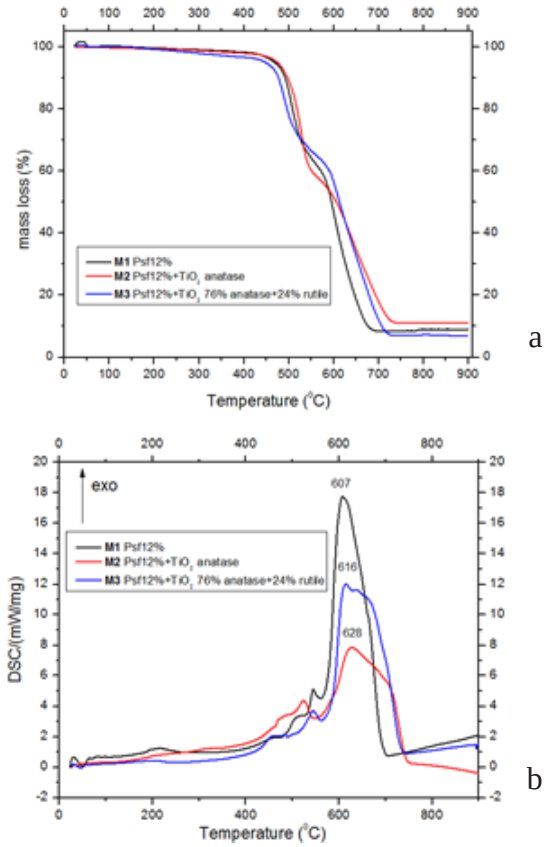

Fig. 5. TG curves (***a***) and DSC curves (*b*) for membranes **M1-M3**

of a thicker skin layer with more TiO_2 NPs concentrated in top layer of the membrane as compared to **M2.**

Energy dispersive X-ray spectroscopy, used in conjunction with SEM, confirmed that the TiO_2 NPs were incorporated into the Psf casting suspension as indicated by the spectral lines of Ti (from TiO_2) at 4.51 keV and 4.94 keV for **M2** (Psf 12% + TiO_2 anatase) (fig. 7, **M2** (b)) and at 4.50 keV and 4.97 keV for **M3** (Psf 12% + TiO_2 76% anatase + 24% rutile) (fig. 7, **M3** (b)).

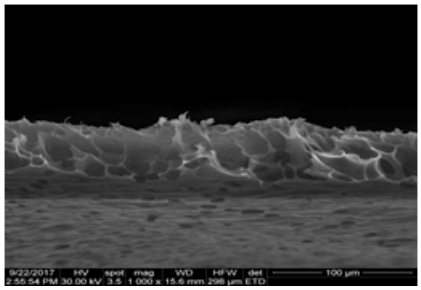

Fig. 6. SEM micrograph of transversal section through **M1** (Psf 12%) membrane

Contact angle measurements

Contact angle measurements confirmed that the polysulfone modified with TiO_2 NPs has an improved hydrophilicity. The contact angle (degrees) of the reference membrane **M1** (Psf 12%) was determined as 83.4±1.6 and, when TiO_2 NPs have been added to the blending mixture, the contact angle decreased to 66.09±5.2 for **M2** (Psf 12% + TiO_2 anatase) and to 65.4±0.3 for **M3** (Psf 12% + TiO_2 76% anatase + 24% rutile).

M3 (Psf 12% + TiO_2 76% anatase + 24% rutile) showed to be the most hydrophilic membrane as compared to **M1** (Psf 12%) and **M2** (Psf 12% + TiO_2 anatase) membranes, and this fact can be assigned to the largest concentration in hydrophilic TiO_2 NPs on the **M3** membrane surface as revealed by SEM images.

Dead-end and cross-flow experiments

The influence of TiO_2 NPs addition into composite membranes upon pure water permeability has been evaluated in ultrafiltration (UF) experiments: dead-end (DE) and cross-flow (CF) filtration modes.

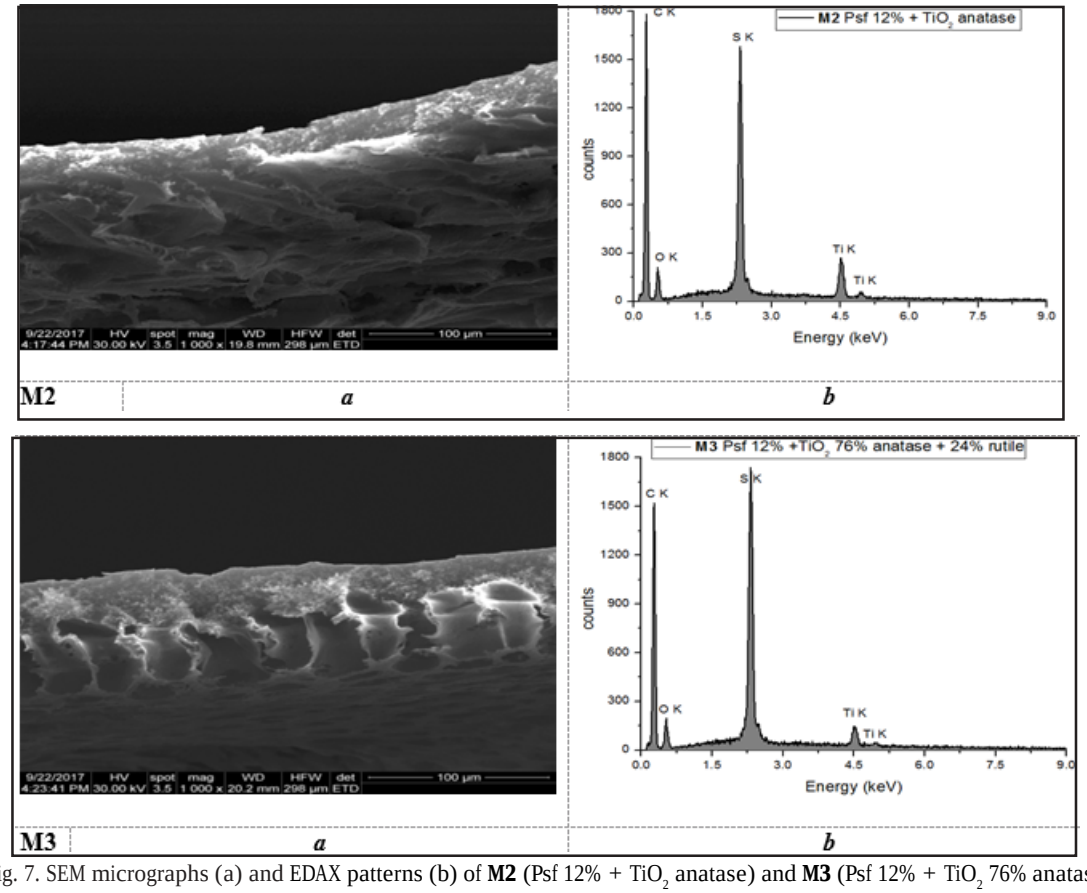

Fig. 7. SEM micrographs (a) and EDAX patterns (b) of **M2** (Psf 12% + TiO_2 anatase) and **M3** (Psf 12% + TiO_2 76% anatase + 24% rutile) membranes

Pressure (bar)	J (L/m^2·h)					
	M1 (Psf 12%)		**M2** (Psf 12% + TiO_2 anatase)		**M3** (Psf 12% + TiO_2 76% anatase+ 24% rutile)	
	DE	**CF**	**DE**	**CF**	**DE**	**CF**
0.5	781.6	123.8	310.2	163.7	294.7	124.5
1.0	728.6	265.3	477.9	276.3	354.7	179.3
2.0	1046.9	717.9	700.4	535.9	340.1	264.1
2.5	930.2	572.9	736.8	643.1	384.4	291.6
3.0	905.4	550.0	768.9	721.8	377.1	305.4

Table 1
WATER FLUX VALUES FOR **M1-M3** MEMBRANES IN DEAD-END AND CROSS-FLOW EXPERIMENTS

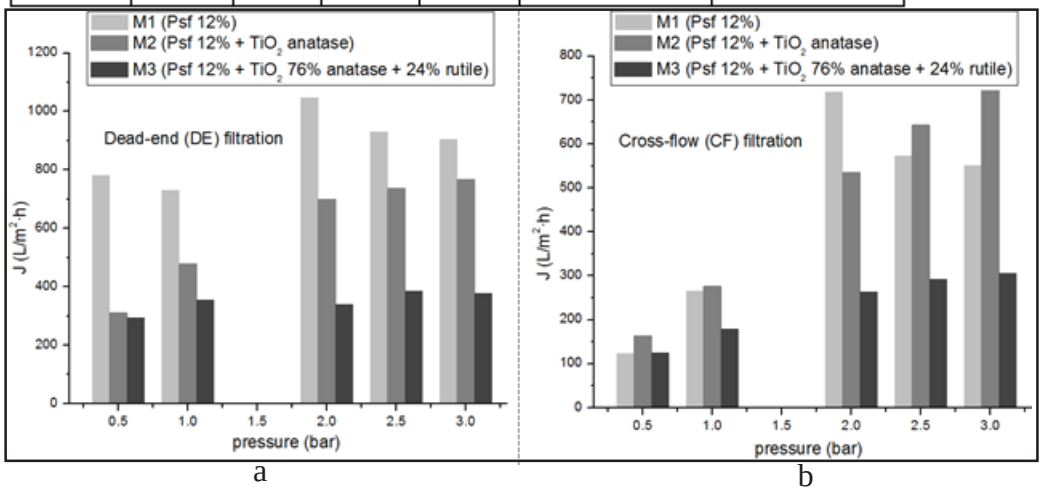

a b

Fig. 8. Water flux of **M1** (Psf 12%), **M2** (Psf 12% + TiO_2 anatase), **M3** (Psf 12% + TiO_2 76% anatase+ 24% rutile) membranes; dead-end (***a***) and cross-flow filtration (***b***)

As shown in Table 1 and figure 8, water permeability measurements showed a decrease of the pure water flux through **M2** (Psf 12% + TiO_2 anatase) and **M3** (Psf 12% + TiO_2 76% anatase+ 24% rutile) membranes in comparison with **M1** (Psf 12%) membrane, used as reference.

Even though the hydrophilicities of **M2** (Psf 12% + TiO_2 anatase) and **M3** (Psf 12% + TiO_2 76% anatase+ 24% rutile) membranes are higher than that of **M1** (Psf 12%), the water flux significantly decreases as a consequence of the nanoparticle skin barrier of the **M2-M3** asymmetric membranes.

However, some important aspects can be pointed out:

- Compared to the **M1** membrane which have a greater flux in dead-end filtration mode, reaching the highest value for 2 bar and then decreasing as the pressure increases, the **M2-M3** membranes have optimal performances at high filtration pressures, 3 bar for both dead-end and cross-flow mode.

- Improved mechanical properties and the relative large water flux measured for **M2-M3** in cross-flow filtration experiments, make these membranes appropriate for ultrafiltration processes.

- At the same time, the improved hydrophilicities of the **M2-M3** membranes are effective for enhancing the fouling resistance and the membranes useful life.

Conclusions

In this work, TiO_2 NPs-Psf composite membranes: **M1** (Psf 12%), **M2** (Psf 12% + TiO_2 anatase), **M3** (Psf 12% + TiO_2 76% anatase+ 24% rutile) have been prepared by phase-inversion method. FTIR and UV-Vis spectra and PXRD analysis confirmed the synthesis of TiO_2 NPs and their estimated diameters were ~21 nm for anatase and ~34 nm/~51 nm for mixed phase 76% anatase/24% rutile.

The morphologies and properties of the composite membranes have been significantly affected

by adding TiO_2 NPs of different sizes to the polymer casting suspension. The hydrophilicity and mechanical and thermal stability are enhanced by incorporating the TiO_2 NPs in membranes. Contact angle measurements confirmed that when the polysulfone was modified with TiO_2 NPs, the hydrophilicity of the membranes increased in the order : 83.4° for **M1** (Psf 12%) < 66.09° for **M2** (Psf 12% + TiO_2 anatase) < 65.4° for **M3** (Psf 12% + TiO_2 76% anatase+ 24% rutile).

Water permeability experiments (dead-end and cross-flow filtration) showed that the TiO_2 NPs-Psf membranes: **M2** (Psf 12% + TiO_2 anatase), **M3** (Psf 12% + TiO_2 76% anatase+ 24% rutile) are suitable for use in ultrafiltration process, the water flux values are 721.83 L/m^2·h for **M2** and 305.4 L/m^2·h for **M3** in cross-flow filtration experiments at pressure of 3 bar.

Acknowledgements: Authors gratefully acknowledge financial support from the Romanian Ministry of European Funds through the Financial Agreements POSDRU/159/1.5/S/132395 and POSDRU/159/1.5/S/134398.

References

1.HOMAYOONFAL, M., MEHRNIA, M.R., MOJTAHEDI, Y.M., ISMAIL, A.F., Desalin. Water Treat., **51**, 2013, p. 3295.
2.PENDERGAST M.M., HOEK, E.M.V., Energy Environ. Sci., **4**, 2011, p. 1946.
3.RIKABI, A.A.K.K., CUCIUREANU, A., CHELU, M., MIRON, A.R., ORBECI, C., POPA, A.G., CRACIUN, M.E., Rev. Chim. (Bucharest), **66**, no. 8, 2015, p. 1093
4.LI, J.G., ZHAO, T.T., CHEN, T.K., LIU, Y.B., ONG, C.N., XIE, J.P., Nanoscale, **7**, 2015, p. 7502.
5.THATAI, S., KHURANA, P. BOKEN, J., PRASAD, S., KUMAR, D., Microchem. J., **116**, 2014, p. 62.

6.AMIN, M.T., ALAZBA, A.A., Membr. Water Treat., **5**, no. 2, 2014, p. 123.
7.MOHMOOD, I., LOPES, C.B., LOPES, I., AHMAD I., DUARTE, A.C., PEREIRA, E., Environ. Sci. Pollut. Res., **20**, 2013, p. 1239.
8.KUMAR, S., AHLAWAT, W., BHANJANA, G., HEYDARIFARD, S., MNAZHAD, M., DILBAGHI, N., J. Nanosci. Nanotechnol., **14**, 2014, p. 1838.
9.GHASEMZADEH, G., MOMENPOUR, M., OMIDI, F., HOSSEINI, M.R., AHANI, M., BARZEGARI, A., Front. Environ. Sci. Eng., **8**, 2014, p. 471.
10.AHMED, T., IMDAD, S., YALDRAM, K., BUTT, N.M., PERVEZ, A., Desalin. Water Treat., **52**, 2014, p. 4089.
11.YIN, J. , DENG, B., J. Membr. Sci., **479**, 2015, p. 256.
12.HOMAYOONFAL, M., MEHRNIA, M.R., MOJTAHEDI, Y.M., ISMAIL, A.F., Desalin. Water Treat., **51**, 2013, p. 3295.
13.GOH, P.S., NG, B.C., LAU, W.J., ISMAIL, A. F., Sep. Purif. Rev., **44**, 2015, p. 216.
14.RAHIMPOUR, A., MADAENI, S.S., TAHERI, A.H., MANSOURPANAH, Y., J. Membr. Sci., **313**, 2008, p. 158.
15.BAE, T.H., KIM, I.C., TAK, T.M., J. Membr. Sci., **275**, 2006, p. 1.
16.LI, J.H., XU, Y.Y., ZHU, L.P., WANG, J.H., DU, C.H., J. Membr. Sci., **326**, 2009, p. 659.
17.MANSOURPANAH, Y., MADAENI, S.S., RAHIMPOUR, A., FARHADIAN, A., TAHERI, A.H., J. Membr. Sci., **330**, 2009, p. 297.
18.BAE, T.H., TAK, T.M., J. Membr. Sci., **249**, 2005, p. 1.
19.RAZMJOU, A., MANSOURI, J., CHEN, V., J. Membr. Sci., **378**, 2011, p. 73.
20.BAE, T.H., TAK, T.M., J. Membr. Sci., **266**, 2005, pp. 1.
21.KWAK, S.Y., KIM, S.H., KIM, S.S., Environ. Sci. Technol., **35**, 2001, p. 2388.
22.MADAENI, S.S., GHAEMI, N., J. Membr. Sci., **303**, 2007, p. 221.
23.OH, S.J., KIM, N., LEE, Y.T., J. Membr. Sci., **345**, 2009, p. 13.
24.BET-MOUSHOUL, E., MANSOURPANAH, Y., FARHADI, K., TABATABAEI, M., Chem. Eng. J., **283**, 2016, p. 29.
25.LI, J.F., XU, Z.L., YANG, H., YU, L.Y., LIU, M., Appl. Surf. Sci., **255**, 2009, p. 4725.
26.WUA, G., GAN, S., CUI, L., XU, Y., Appl. Surf. Sci., **254**, 2008, p. 7080.
27.SOROKO, I., LIVINGSTON, A., J. Membr. Sci., **343**, 2009, p. 189.
28.LI, J.B., ZHU, J.W., ZHENG, M.S., J. Appl. Polym. Sci., **103**, 2007, p. 3623.
29.YU, L.Y., XUA, Z.L., SHEN, H.M., YANG, H., J. Membr. Sci., **337**, 2009, p. 257.
30.LEE, H.S., IM, S.J., KIM, J.H., KIM, H.J., KIM, J.P., MIN, B.R., Desalination, **219**, 2008, p. 48.
31.LUO, M.L., ZHAO, J.Q., TANG, W., PU, C.S., Appl. Surf. Sci., **249**, 2005, p. 76.
32JYOTHI, M.S., NAYAK, V., PADAKI, M., BALAKRISHNA, R.G., ISMAIL, A.F., Desalination, **354**, 2014, p. 189.
33.JYOTHI, M.S., NAYAK, V., PADAKI, M., BALAKRISHNA, R.G., SOONTARAPA, K., Chem. Eng. J., **283**, 2016, p.1494.
34.YANG, Y., ZHANG, H., WANG, P., ZHENG, Q., LI, J., J. Membr. Sci., **288**, 2007, p. 231.
35.YANG, Y., WANG, P., ZHENG, Q., J. Polym. Sci. B: Polym. Phys., **44**, 2006, p. 879.
36.YANG, Y., WANG, P., Polymer, **47,** 2006, p. 2683.
37.HAMID, N.A.A., ISMAIL, A.F., MATSUURA, T., ZULARISAM, A.W., LAU, W.J., YULIWATI, E., ABDULLAH, M.S., Desalination, **273**, 2011, p. 85.
38.CAO, X., MA, J., SHI, X., REN, Z., Appl. Surf. Sci., **253**, 2006, p. 2003.
39.NGAMTA, S., BOONPRAKOB, N., WETCHAKUN, N., OUNNUNKAD, K., PHANICHPHANT, S., INCEESUNGVORN, B., Mater. Lett., **105**, 2013, p. 76.
40.PATTERSON, A., Phys. Rev., **56(10)**, 1939, p. 978.
41.KESTING, R.E., Synthetic polymeric membranes: a structural perspective, Wiley-Interscience, New York, **1985.**
42.POPESCU, G., NECHIFOR, G., ALBU, B., LUCA, N., Rev. Roum. Chim., **34**, no. 2, 1989, p. 577.
43.CUCIUREANU, A., BATRINESCU, G., BADEA, N.N., RADU, D.A., NECHIFOR, G., Mat. Plast., **47**, no. 4, 2010, p. 416.
44.NECHIFOR, G., VOICU, S.I., NECHIFOR, A.C., GAREA, S., Desalination, **241**, no. 1-3, 2009, p. 342.
45.VOICU, S.I., STANCIU, N.D., NECHIFOR, A.C., VAIREANU, D.I., NECHIFOR, G., Romanian Journal of Information Science and Technology, **12**, no.3, 2009, p. 410.
46.POPA, G.A., POPA (ENACHE), D.F., SLAVE(CLEJ), D.D., DIN, I.S., MIREA, C.M., CIOCANEA, A., Rev. Chim. (Bucharest), **68**, no. 1, 2017, p. 6.
47.RIKABI, A.A.K.K., NECHIFOR, A.C., MOHAMMED, T. J., OPREA, O., MIRON, A.R., SEGARCEANU, M., VAIREANU, D.I., Rev. Chim. (Bucharest), **67**, no. 8, 2016, p. 1489.
48.RIKABI, A.A.K.K., BALABAN (CHELU), M., HARABOR, I., ALBU, P.C., SEGARCEANU, M., NECHIFOR, G., Rev. Chim. (Bucharest), **67**, no. 9, 2016, p. 1658.
49.AL ANI, H.N.A., CIMBRU, A.M., TRISCA-RUSU, C., TANCZOS, S.K.., CUCIUREANU, A., NECHIFOR, A.C., Rev. Chim. (Bucharest), **68**, no. 2, 2017, p. 203.
50.AL ANI, H.N.A., CIMBRU, A.M., TANCZOS, S.K.., DIN, I.S., CUCIUREANU, A., NAFLIU, I.M., NECHIFOR, G., Rev. Chim. (Bucharest), **68**, no. 3, 2017, p. 427.
51.BATRINESCU, G., CONSTANTIN, M.A., CUCIUREANU, A., NECHIFOR, G., Polymer Engineering and Science, **54**, no. 7, 2014, p. 1640.

Manuscript received: 3.05.2017